Geophysical Research Letters

RESEARCH LETTER
10.1029/2018GL081577

Seasonality and Buoyancy Suppression of Turbulence in the Bay of Bengal

Ritabrata Thakur[1], **Emily L. Shroyer**[2], **Rama Govindarajan**[1], **J. Thomas Farrar**[3], **Robert A. Weller**[3], **and James N. Moum**[2]

[1]International Centre for Theoretical Sciences, Tata Institute of Fundamental Research, Bengaluru, Karnataka, India, [2]College of Earth, Ocean, and Atmospheric Sciences, Oregon State University, Corvallis, OR, USA, [3]Woods Hole Oceanographic Institution, Woods Hole, MA, USA

Key Points:
- Upper-ocean turbulence in the Bay of Bengal is quantified using yearlong moored data
- Turbulence above 25 m was directly related to wind forcing throughout most of the year
- After SW monsoon surface low-salinity water suppressed turbulence below 25 m for 3–5 months

Supporting Information:
- Supporting Information S1

Correspondence to:
R. Thakur,
ritabrata.thakur@icts.res.in

Citation:
Thakur, R., Shroyer, E. L., Govindarajan, R., Farrar, J. T., Weller, R. A., & Moum, J. N. (2019). Seasonality and buoyancy suppression of turbulence in the Bay of Bengal. *Geophysical Research Letters*, *46*, 4346–4355. https://doi.org/10.1029/2018GL081577

Received 4 DEC 2018
Accepted 3 APR 2019
Accepted article online 8 APR 2019
Published online 23 APR 2019

Abstract

A yearlong record from moored current, temperature, conductivity, and four mixing meters (χpods) in the northernmost international waters of the Bay of Bengal quantifies upper-ocean turbulent diffusivity of heat (K_t) and its response to the Indian monsoon. Data indicate (1) pronounced intermittency in turbulence at semidiurnal, diurnal, and near-inertial timescales, (2) strong turbulence above 25-m depth during the SW (summer) and NE (winter) monsoon relative to the transition periods (compare $K_t > 10^{-4}$ m^2/s to $K_t \sim 10^{-5}$ m^2/s, and (3) persistent suppression of turbulence ($K_t < 10^{-5}$ m^2/s) for 3 to 5 months in the latter half of the SW monsoon coincident with enhanced near-surface stratification postarrival of low-salinity water from the Brahmaputra-Ganga-Meghna delta and monsoonal precipitation. This suppression promotes maintenance of the low-salinity surface waters within the interior of the bay preconditioning the upper northern Indian Ocean for the next year's monsoon.

Plain Language Summary

Fluctuations in the intensity of the Indian monsoon system propagate northward from the equator toward the Indian subcontinent, bringing intervals of relatively wet and dry conditions. Rains both feed many rivers that discharge into the northern Bay of Bengal and provide close to 2 m of rainfall over the basin. The freshwater persists as a shallow layer in the bay for 3–5 months starting around July (the latter half of the summer monsoon). This shallow, freshwater layer adjusts quickly to changes in air-sea heat fluxes but also limits atmospheric forcing of the ocean below. Our yearlong data set quantifies upper-ocean turbulent mixing in the northern bay. Above 25 m, we find that (1) mixing is very strong during the summer monsoon (June–September) due to the strong winds, (2) mixing is reduced from summer monsoon values during the winter monsoon (November–January), and (3) mixing is lowest during transition periods between the two. The ocean responds differently below 25 m. The freshwater layer on top acts as a barrier to the winds, and mixing is suppressed for several months. Below 60 m, even an intense cyclone could not generate appreciable ocean mixing when the freshwater layer was present.

1. Introduction

Modeling studies have shown that the coupled dynamics of the ocean-atmosphere system, at timescales as short as the diurnal, strongly affect the structure and variability of the large-scale tropical atmosphere (Fu et al., 2003; Inness & Slingo, 2003; Woolnough et al., 2007). Observations have further demonstrated the coevolution of the atmosphere and ocean in response to monsoon forcing in the Indian Ocean, including within the Madden-Julian Oscillation (McPhaden & Foltz, 2013; Moum et al., 2014, 2016), and during boreal summer intraseasonal oscillations (Li et al., 2017; Sengupta & Ravichandran, 2001). While sea surface temperature (SST) controls coupling at the air-sea interface, SST is itself influenced by net atmosphere-ocean heat flux, turbulent entrainment of typically cooler deep water into the mixed layer (ML), horizontal and vertical advection, and the ocean's mixed layer depth (MLD).

The Bay of Bengal (BoB) has the lowest-salinity surface waters in the tropical ocean due to numerous rivers discharging into it (Sengupta et al., 2006) and heavy local seasonal precipitation (Hoyos & Webster, 2007). Southward spreading low-salinity water from the world's largest delta, the Brahmaputra-Ganga-Meghna (Sengupta et al., 2016), peaks during July–September (Papa et al., 2010). The low-salinity surface water and consequent shallow MLDs make the BoB an "active communicator" with the atmosphere (Bhat et al., 2001), with potential consequence to the Indian monsoon system (Rajeevan et al., 2010; Sengupta & Ravichandran,

2001), and synoptic convective activities (Balaguru et al., 2014). Studies have shown the local dispersion mechanisms (Sree Lekha et al., 2018) and the exit pathways of this low-salinity water from the BoB (Jensen, 2003; Sengupta et al., 2006; Shetye et al., 1996). However, the role of this low-salinity water in modulating diapycnal mixing has not yet been addressed.

Salinity often dominates stratification at the base of the ML in the BoB, allowing for formation of a barrier layer defined as the region between the base of the ML and the deeper thermocline. Strong salinity stratification also allows for multiple fine-scale (<10 m) inversions in temperature and persistent subsurface warm layers (Shroyer et al., 2016). These features provide an additional reservoir of heat, which may influence SST; for example, tropical cyclones within the BoB have been known to leave a salty but not a pronounced cool wake because of this subsurface heat (Chaudhuri et al., 2019; Girishkumar et al., 2014; Jourdain et al., 2013). Long-term turbulence measurements provide the opportunity to explore how turbulence influences the upper-ocean structure within the context of the BoB's evolving stratification (due to precipitation and riverine discharge) and monsoon forcing.

Moored mixing meters (χpods; Moum & Nash, 2009) have made it possible to resolve multiyear subsurface turbulence at sites across the globe (Moum et al., 2013; Perlin & Moum, 2012; Pujiana et al., 2018; Warner et al., 2016). Warner et al. (2016) studied the seasonality in turbulence in the BoB for the first time from a single χpod at 15-m depth at 12° N. This study found that the turbulent heat fluxes were of similar magnitude to the surface flux during the monsoon (stronger wind) periods, whereas it was 3 orders of magnitude weaker during the transition (weaker wind) periods. In the present study, we examine results from four χpods (at depths ranging from 22 to 65 m) on a heavily instrumented upper-ocean mooring in the northern BoB (18° N). These data capture the development of intense, persistent (multiple months) near-surface stratification and shallow MLs associated with the advective arrival of low-salinity water from riverine discharge and rainfall. During this time, salinity contributed three to five times the magnitude of temperature to upper-ocean density stratification, supporting formation of a thin but intense barrier layer. These data provide direct evidence on the role of low-salinity water in controlling the depth of penetration of turbulent mixing in the northern BoB. A remarkable suppression of turbulence below 40 m is seen even during periods of strong winds including a cyclone when this low-salinity water existed on the surface.

2. Data and Methods

An oceanographic mooring with surface sensors was deployed in the northernmost international waters of the BoB (18° N, 89.5° E) from 8 December 2014 to 29 January 2016 to record oceanic and atmospheric data (Weller et al., 2016, 2018). Thirteen Sea-Bird Electronics 37-SM MicroCATs from 2.5 to 95 m logged conductivity (C) and temperature (T) every 5 min while two of them at 1-m depth sampled C and T every minute, and several also recorded pressure. We infer salinity and density from C and T (McDougall & Barker, 2011). An upward-looking Teledyne RD Instruments 300-kHz acoustic Doppler current profiler was deployed at 80 m and sampled 2-m bins from 74.5 m upward. Data from a meteorological package (ASIMET; Hosom et al., 1995) were used to approximate the air-sea fluxes with bulk formulae (Fairall et al., 2003).

Six χpods were deployed from 22 to 65 m; one was lost at sea, and a second returned data for only half of the deployment. Here we analyze data from the remaining four χpods deployed at 22, 46, 55, and 65 m. χpods record temperature using fast thermistors, current speed (u) with Pitot tubes (Moum, 2015), pressure, and acceleration at 50 Hz. The time rate of temperature change (T_t) is measured at 100 Hz, and compass heading is sampled at 1 Hz. Taylor's frozen flow hypothesis (Taylor, 1938) is used to map time derivative (T_t) to spatial derivative (T_x), as $T_x = T_t/u$. An iterative algorithm (Moum & Nash, 2009) is used to determine the decay rate of temperature variance (χ; Figure S1 in the supporting information) using an inferred turbulent kinetic energy dissipation rate (ϵ_χ), as $\epsilon_\chi = \frac{N^2\chi}{2\Gamma T_z^2}$, to estimate the Batchelor wave number. Here T_z is the mean vertical temperature gradient and $N^2 = -g\rho \cdot d\rho/dz$, where ρ is the fluid density. Γ is related to the efficiency of turbulent mixing and was first argued to be approximately 0.2 by Osborn (1980); see also Gregg et al. (2018) and Smyth et al. (2001). Estimates of χ are calculated on 1-s intervals, and the turbulent diffusivity for heat (hereafter diffusivity) is calculated as $K_t = \frac{\chi}{2T_z^2}$ (Osborn & Cox, 1972), using 10-min averages of χ and the mean temperature gradient. Sensitivity of χ to changes in Γ is given in the appendix of Moum and Nash (2009); see also Supporting Information S1. K_t is not evaluated when $|T_z| < 10^{-3}$ °C/m, or when $N^2 < 10^{-6}$ s^{-2} to preclude estimates during periods of convection and weak stratification. Based on these criteria, 7.5% (<1.5%) of the 1-s χ estimates are flagged from the 22-m χpod (other three χpods). Short

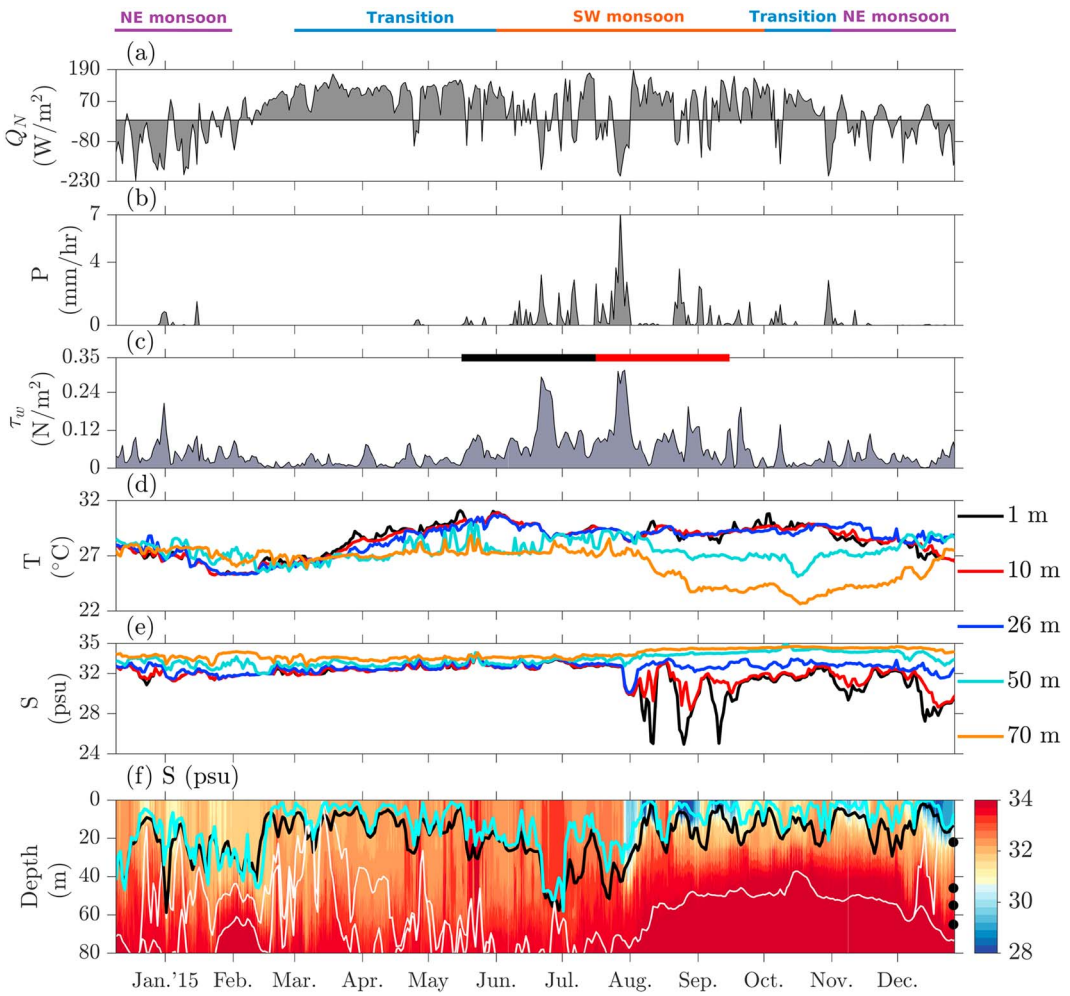

Figure 1. Daily-averaged (a) net surface heat flux Q_N (positive is heat going into the ocean at surface); (b) precipitation **P**; (c) wind stress τ_w (black and red indicate periods shown in Figure 2); (d/e) temperature **T**/salinity **S** at 1 (sea surface temperature), 10, 26, 50, and 70 m. (f) **S** in color with the temperature-based mixed layer depth (black), density-based mixed layer depth (cyan), 27 °C isotherms (white) overlaid, and χpod deployment depths (black circles). The climatologically averaged Indian monsoon cycle is indicated above (a).

spectral windows applied in calculation of χ avoid contamination by surface waves, and 10-min estimates of K_t average over any surface-wave signal (see also Supporting Information S1).

The most recent χpod configuration is described in Becherer and Moum (2017). Detailed comparisons of turbulence estimates from χpods and more traditional shear microstructure profilers are discussed in Perlin and Moum (2012) and Pujiana et al. (2015).

3. The Indian Monsoon of 2015

At the mooring location, the 2015 winter or northeast (NE) monsoon was characterized by negative net surface heat flux that acted to cool the ocean with seasonal-average of −51.4 W/m^2 (daily values peaked at −229 W/m^2; Figure 1a), occasional precipitation (daily values ranged 0.2–1.5 mm/hr; Figure 1b), and strong, persistent northeasterly winds (daily stress peaked at 0.2 N/m^2; Figure 1c). In contrast, the 2015 winter-summer transition period was characterized by positive net surface heat flux in excess of 120 W/m^2 (peaking at 170 W/m^2), negligible precipitation (<0.3 mm/hr), and low wind stress (<0.04 N/m^2). During this transition, surface air temperature increased from 24 ° C in February to 31 ° C in June. The summer or southwest (SW) monsoon was characterized by fluctuating net surface heat flux and a decrease in surface air temperature to 28 ° C by September, persistent and heavy precipitation events (>2mm/hr), and the strongest observed variability in wind stress, for example, 0.01–0.1 N/m^2 during 15–23 May and 0.04–0.3 N/m^2 during

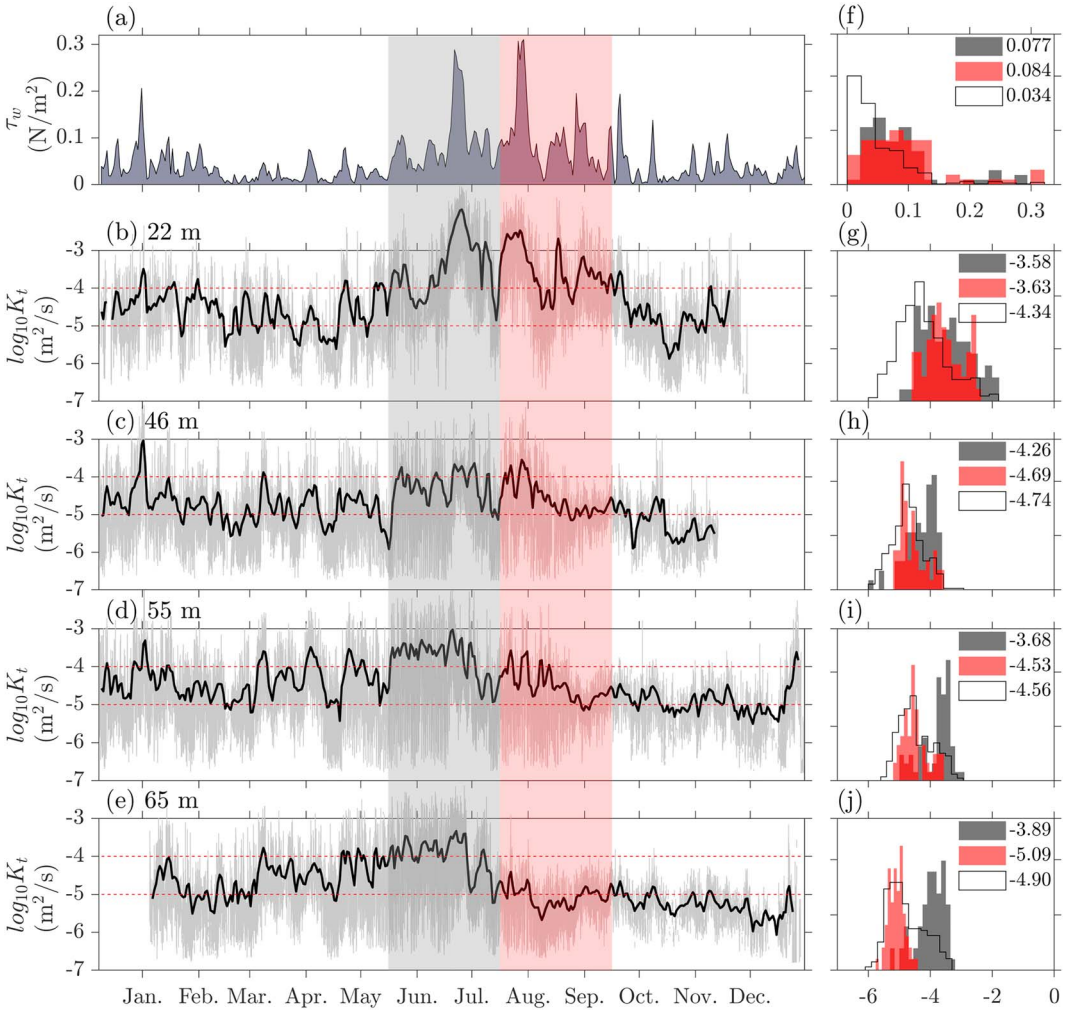

Figure 2. (a) Daily-averaged wind stress τ_w. Daily-averaged diffusivity $log_{10}K_t$ at (b) 22 m, (c) 46 m, (d) 55 m, and (e) 65 m in black, and smoothed 1-min averages in gray. (f) Normalized histograms of daily-averaged τ_w for 15 May to 15 July (gray), 15 July to 15 September (red), and the whole year (black outline). (g-j) Normalized histograms of daily-averaged $log_{10}K_t$ at same depths as (b)–(e) and color coding similar to (a) and (f). Median values are indicated in (f)–(j).

16–21 June. Cyclone *Komen* in late-July is identified by its associated negative net surface heat flux and the year's highest precipitation and wind stress.

Upper-ocean temperatures (Figure 1d) increased during the transition to SW monsoon, resulting in increased stratification over the upper 70 m. In June, they reached peak values after which the upper 25 m cooled by almost 2.5 ° C over a 1-month period in concert with increasing monsoon winds. The onset of SW monsoon winds was coincident with a shoaling of deep isopycnals in July/August, which later deepen again in December (Figures 1d–1f). The general timing of uplifting (lowering) of isopycnals is consistent with the transition to positive (negative) wind stress curl in the northern BoB based on wind climatology (Risien & Chelton, 2008). This signal may be associated with upwelling (downwelling), but its origin is not certain, given uncertainties associated with the interpretation of large-scale gradients past mooring sensors.

Substantial decreases in salinity (>6 psu; Figures 1e and 1f) during the latter half of the SW monsoon mark the arrival of waters modified by Brahmaputra-Ganga-Meghna discharge and precipitation. The first low-salinity pool arrived on 29 July accompanied by ~0.5 ° C drop in SST. Subsequent shallow (<15 m), low-salinity (<27 psu) pools appeared over the SW monsoon persisting for roughly 10 days. Very shallow MLDs (less than 10 m deep) were associated with these features (temperature-based MLD defined by $|T_{ML} - \mathrm{SST}| \leq 0.15$ ° C and the density-based MLD defined following Lorbacher et al. (2006); Figure 1f). Low-salinity

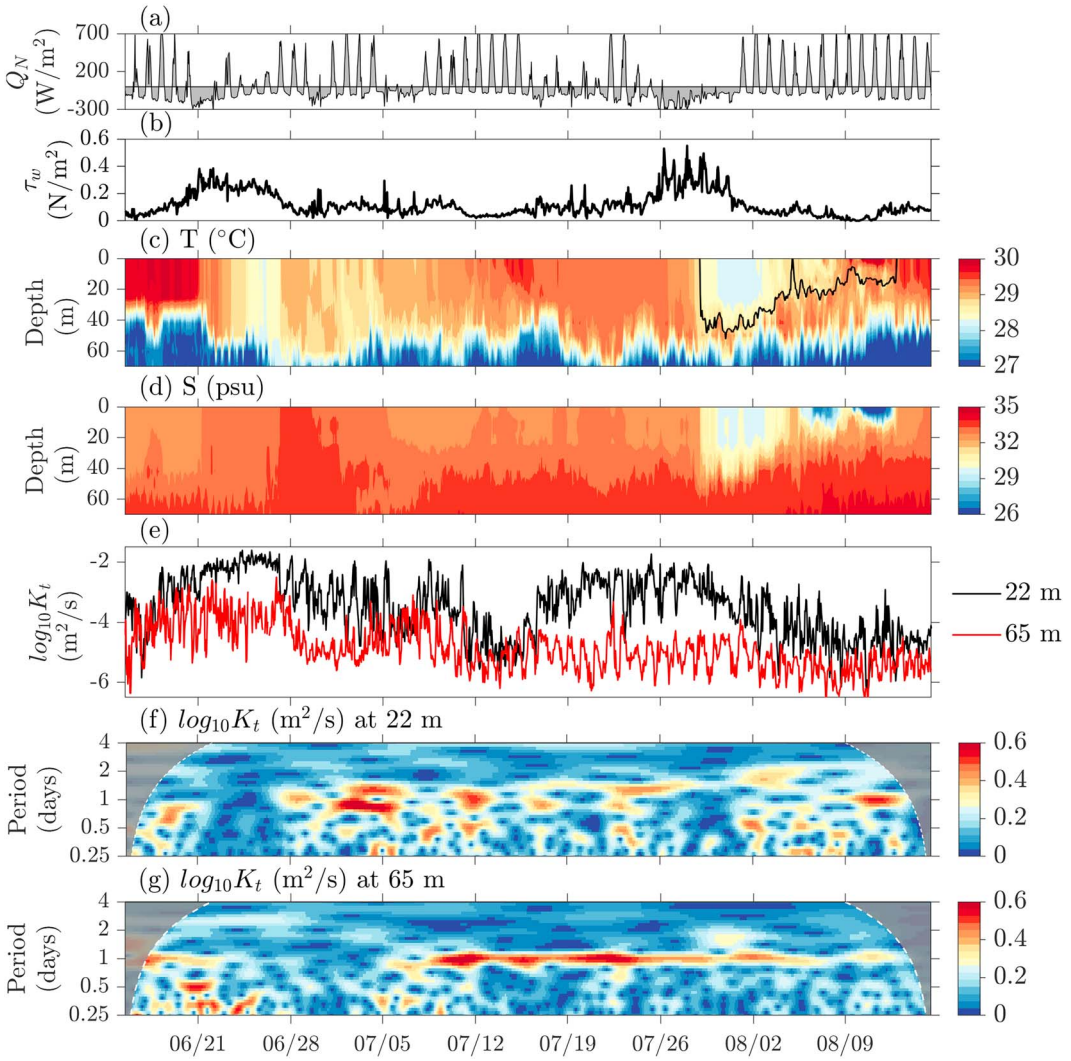

Figure 3. Hourly-averaged (a) net surface heat flux Q_N, (b) wind stress τ_w, (c) temperature **T** (black line is the 32-psu isohaline), (d) salinity **S**, and (e) diffusivity $log_{10}K_t$ at 22 and 65 m. Wavelet transforms of $log_{10}K_t$ at (f) 22 m and (g) 65 m.

features observed later in the year (November and December) show similarly shallow MLDs. The barrier layer thickness (i.e., difference between the density and temperature MLDs) was on average 8.5 m and peaked at roughly 20 m in the latter half of the SW monsoon.

4. Observed Upper-Ocean Turbulence

Interpretation of turbulence measurements from these four moored χpods requires resolution of the MLD. The ML was nearer to the 22-m χpod for a significant portion of the year (Figure 1f). Responding to >0.24 N/m^2 wind stress events in the SW monsoon, the ML extended below the 46-m χpod for a total of 13 days. The diffusivity indicates variability in turbulence both above and below the ML over a wide range of timescales (Figure 2). The characteristics of turbulence differed based on whether or not the χpod was near the base of the ML (22-m χpod; Figures 1f, 2b, and 2g) or below the ML (other three χpods; Figures 1f, 2c–2e, and 2h–2j), as the interplay of surface forcing and stratification differed within these two environments. One manifestation of this difference is that turbulence at 22 m tended to be stronger in magnitude and different in frequency than the sub-ML (>40 m) turbulence. The difference is primarily attributed to the SW monsoon when the median (mean) value of the 22-m diffusivity was 1 (3) order(s) of magnitude higher than the sub-ML diffusivity.

Although intermittent, variability in turbulence at diurnal, semidiurnal, and shorter timescales is observed below the ML; these signals were particularly enhanced within the diurnal band during the transition and the SW monsoon (Figures 3 and S2). For example, at 65 m, a persistent (~1 month) diurnal signal in diffusivity ranging 2 orders of magnitude is seen through the majority of July (Figures 3e and 3g), coincident with a period of increased subsurface stratification. This intermediate-depth diurnal signal in diffusivity is also seen at 46 and 55 m, but it is not as persistent (<15 days) as at 65 m. In contrast, the 22-m diffusivity shows a broadband variability at the diurnal timescale (Figures 3e and 3f). Recall that estimates of χ are not calculated during convective periods. This omission combined with the lack of a convincing propagation from the surface suggests that the diurnal signal is not convective in origin.

The origin of the diurnal cycle in diffusivity is not entirely clear and is a topic of further exploration. A few noteworthy points, (1) the diurnal signal in diffusivity is narrowband (Figure S3), (2) the internal tide signal (as diagnosed with band-passed, depth-dependent velocity; not shown) has a stronger semidiurnal component (energy density ~10 J/m^3) than diurnal (energy density <5 J/m^3), and (3) a strong diurnal signal in temperature stratification is not seen during this time period (Figure S3; e.g., as would be anticipated for the development of a diurnal jet; Sutherland et al., 2016). A weak narrowband diurnal signal is apparent in the east-west wind stress (Figure S4) during this time, so a possible interpretation is that the signal is in response to acceleration of the water column by the winds. An alternative theory is that layers of enhanced mixing are vertically advected past depth sensors by the diurnal tide. This explanation depends on the vertical scale of stratification, shear, and mixing layers and their location relative to sensors. Observed patterns in shear, stratification, and Richardson number do not yield conclusive evidence of heaving (Figure S5). One final explanation is that the diurnal signal is biological in origin, that is, forced by migrating zooplankton or fish (Pujiana et al., 2015). Given the lack of a narrowband diurnal signal in ancillary physical fields (e.g., stratification and velocity), biogenically forced turbulence is a possibility.

Turbulence also varied at the intraseasonal and seasonal timescales, which is arguably the most obvious feature of Figure 2. For example, the 22-m χpod shows a strong 30-day signal in diffusivity ranging 3 orders of magnitude during the SW monsoon. We distinguish two periods of the SW monsoon, 15 May to 15 July and 15 July to 15 September. These periods were nominally defined by the buildup of the SW monsoon winds (Figure 1c) and similar wind stress distributions (Figures 2a and 2f). Hence, the first period (black rectangle in Figures 1c and 2) represents conditions in the SW monsoon before arrival of low-salinity water, and the second period (red rectangle in Figures 1c and 2) represents conditions in the SW monsoon after arrival of low-salinity water. Despite having similar wind stress, turbulence is quantitatively different in the two periods for the sub-ML χpods.

4.1. Seasonality in Turbulence Near the Base of the ML

Turbulence at 22 m generally followed the strength of the surface winds (Figures 2a, 2b, and S6) with the weakest (strongest) winds and diffusivities observed during the transition (SW monsoon). The median diffusivity during the transition to the SW monsoon was 1.5×10^{-5} m^2/s, which increased to 2.5×10^{-4} m^2/s during the SW monsoon. The highest diffusivity (1.1×10^{-2} m^2/s) is observed during the SW monsoon coincident with wind stress in excess of 0.3 N/m^2 (Figure 3b). The transition to the NE monsoon was associated with lower values of diffusivity (median 1.9×10^{-5} m^2/s; mean 3.8×10^{-5} m^2/s). The distributions of 22-m diffusivity (Figure 2g) prearrival and postarrival of low-salinity water are very similar (median 2.5×10^{-4} m^2/s vs. 2.4×10^{-4} m^2/s) and an order of magnitude higher than the full year (median 4.2×10^{-5} m^2/s). However, diffusivity from mid-September until the end of October was low despite a few high wind stress events.

4.2. Seasonality in Turbulence Below the ML

At the onset of the SW monsoon winds (0.01–0.1 N/m^2 during 15–23 May), diffusivity at 46, 55, and 65 m approached that of the 22 m (1.8×10^{-4} m^2/s on 23 May). (The 46 and 55 m diffusivity increased by roughly an order of magnitude within a few days at this time, while the 65-m diffusivity, already elevated, increased at a slower rate.) Elevated sub-ML diffusivity is also seen during other seasons in response to winds, for example, the peak on 1 January that coincided with a reduction in stratification (Figures 2c and 2d). Diffusivity distributions differ significantly from one another with an increasing shift between median values progressing downward in depth (Figures 2h–2j).

The most pronounced trend in sub-ML turbulence is the steady decline in the intensity and variance of diffusivity observed during the latter half of the SW monsoon and into the NE monsoon season (Figures 2c–2e),

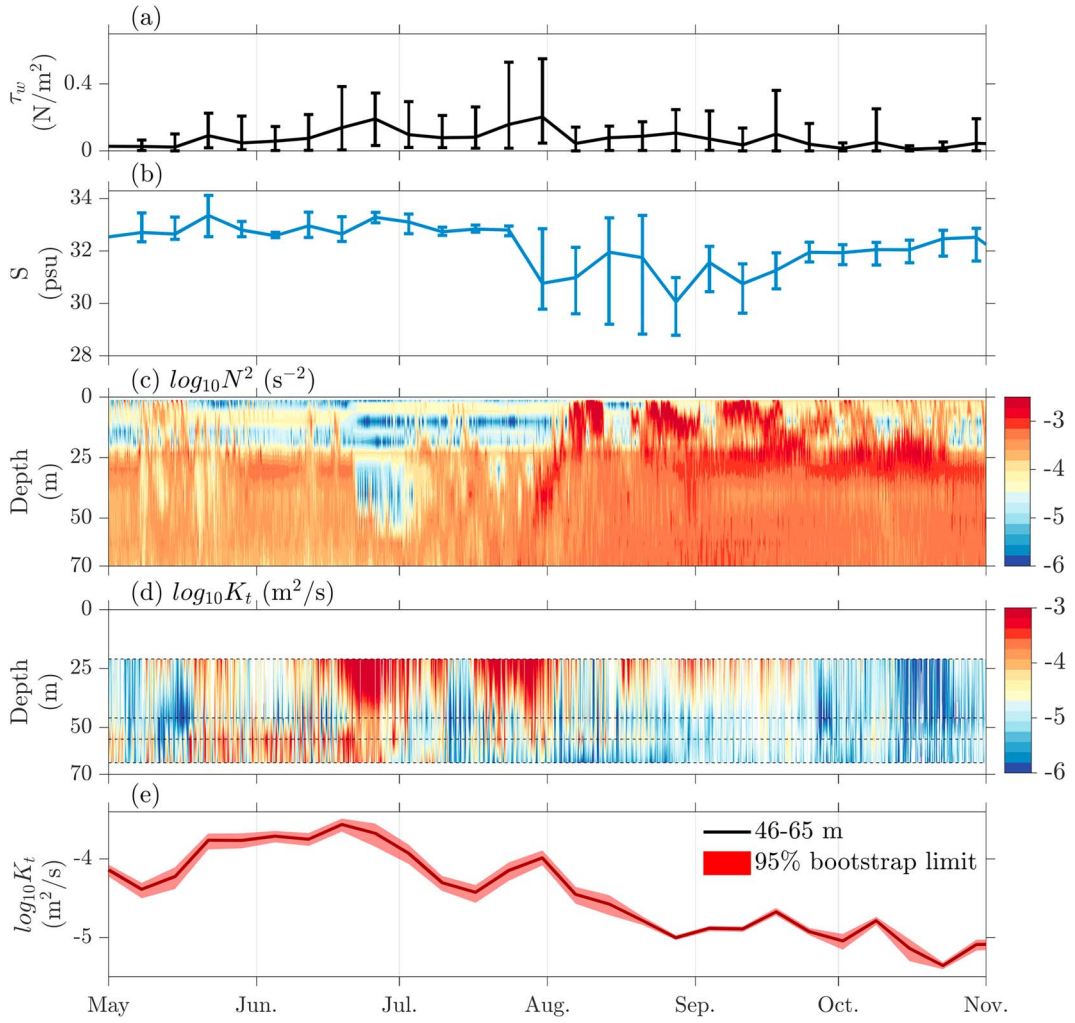

Figure 4. Weekly-averaged (a) wind stress τ_w and (b) upper 30-m salinity **S**, with error bars by maximum and minimum hourly-averaged τ_w and **S** within each week (from hourly averages), respectively. Hourly-averaged (c) $\log_{10}N^2$ and (d) $log_{10}K_t$ interpolated linearly between 22-, 46-, 55-, and 65-m χpod depths (black dotted lines). (e) Weekly-averaged 46- to 65-m $log_{10}K_t$ with the 95% bootstrap limit.

despite strong winds. After this decline, daily median and mean values of diffusivity remained low (10^{-5} – 10^{-6} m^2/s) for 3–5 months.

5. Buoyancy Suppression of Turbulence Below the ML by Low-Salinity Water

The low-salinity water was detected in the mooring in distinct pulses starting late-July and continuing into the early NE monsoon (Figure 1f; the first occurrence is a set of three pools over 2 weeks (Figure 3d). The first pool on 29 July was ~40-m deep, and the next two pools on 5 and 9 August were relatively shallow (~20 m). The first caused an increase in stratification below 25 m while the following two caused increased stratification above 25 m (in both cases $N^2 \sim 10^{-3}$ s^{-2}; Figure 4c). (Note that arrival of these freshwater pools was roughly coincident with shoaling of subsurface isopycnals; however, the near-surface salinity stratification accounted for a majority of the total change in upper-ocean stratification during boreal summer. Both near-surface low-salinity water and the compression of isopycnals at depth contributed significantly to the stratification in boreal fall; Figure S7)

The response of diffusivity to the increase in stratification associated with arrival of low-salinity water must be interpreted with consideration of surface forcing, especially with regard to the strong storms occurring in June and July (wind stress >0.3 N/m^2). The decrease in winds on 28 June and 12 July coincided with reduced diffusivities at all depths (Figures 2, 3b, and 3e).

The reduction in diffusivity over this time span varied from 1.5–3 orders of magnitude in hourly averages for the different χpods (Figure 4d). As compared to the late-June storm, the increase in diffusivity during *Komen* was less in magnitude and restricted only to shallower depths (Figures 4d and 4e). The signal of *Komen* is not at all obvious at 65 m (Figure 3e). This is despite stronger wind stress during *Komen* (*Komen's* storm center passed within ~350 km of the mooring on 29 July.) High wind stress events occurred during August and September, but diffusivities (and their daily ranges) below the ML remained low (Figures 2, 4d, and 4e). After *Komen*, extreme turbulence events (1-min data; Figure 2) rarely exceeded 10^{-4} m^2/s below 45 m. Over this time period, the daily mean diffusivity at 65 m was $\lesssim 10^{-5}$ m^2/s. Closer to the surface (22 m), it ranged between 10^{-3} and 10^{-6} m^2/s.

Weekly averages of wind, salinity, and sub-ML diffusivity reflect the relative correlations between forcing, stratification, and turbulence at this timescale. Weekly-averaged sub-ML diffusivity mimics the weekly averaged surface salinity rather than the wind stress, in that the presence of low-salinity water ($S < 32$ psu; Figure 4b) is associated with reduced diffusivity (Figure 4e) but variable wind forcing (Figure 4a).

6. Conclusions

The upper-ocean turbulent response of the northern BoB is notable in several ways. First, semidiurnal to near-inertial variability in turbulence shows intermittency throughout the year with periods of enhanced turbulence often spanning 1 week to 1 month. The differences and variability at distinct depths (22, 46, 55, and 65 m) are a reflection of the small vertical scale in the stratification (Figure 4c), which is often of the order of 10 m or less. Furthermore, as layers heave past the χpods, signals that persist on individual layers will be interpreted as time variability at that depth.

Second, turbulence within and near the base of the ML (22 m) shows a strong seasonality that varies with monsoon winds, similar to results found by Warner et al. (2016) at 12° N. Turbulent diffusivity was strongest ($>10^{-3}$ m^2/s) in the SW monsoon with the two strongest storms of the year. In contrast to Warner et al. (2016), diffusivity during the NE monsoon of 2015 was weaker than during the SW monsoon at 18° N. During times of weak winds, often during transition periods, the daily averaged diffusivity occasionally dropped below 10^{-5} m^2/s.

Third, turbulence beneath the ML (46–65 m) was suppressed in the second half of the SW monsoon during the period of arrival of low-salinity water from riverine discharge and precipitation (Figures 4b and 4e), coincident increase in near-surface salinity stratification (initial response), and also elevated subsurface temperature stratification (boreal fall). A noteworthy example of this suppression is the lack of turbulent response in the 65-m χpod when cyclone *Komen* transited the northern BoB (Figure 3e). Following *Komen*, turbulence remained suppressed below the ML for 3 to 5 months (Figure 4e). Turbulence at 55 m recovered to its original strength by the end of the year.

For 18° N, the high near-surface stratification contributed significantly to limiting vertical turbulent "communication" within the water column for multiple months, isolating subsurface heat reservoirs with consequences to upper-ocean heat and salt content and air-sea interactions. This suppression of turbulence will also limit storage of surface fluxes at depth and must contribute toward the longevity of the low-salinity surface layer.

Acknowledgments
This work was supported by the U.S. Office of Naval Research (ONR) Grants N00014-14-1-0236 and N00014-17-1-2472, and the Ocean Mixing and Monsoon program of the Indian Ministry of Earth Sciences. The deployment of the Woods Hole Oceanographic Institution mooring and RW and JTF were supported by ONR Grant N00014-13-1-0453. The deployment and recovery of the mooring were carried out by RV Sagar Nidhi and RV Sagar Kanya, respectively, with the help of the crew and science parties. Thanks to National Institute of Ocean Technology (India) for buoy support. The authors acknowledge invaluable discussions with Johannes Becherer, Deepak Cherian, and Sally Warner at CEOAS, OSU, and Dipanjan Chaudhuri, J Sree Lekha, and Debasis Sengupta at CAOS, IISc. The authors thank two anonymous reviewers for their detailed reviews, which have helped sharpen many aspects of this paper. Data can be accessed as described in section S2.

References

Balaguru, K., Taraphdar, S., Leung, L. R., & Foltz, G. R. (2014). Increase in the intensity of postmonsoon Bay of Bengal tropical cyclones. *Geophysical Research Letters*, *41*, 3594–3601. https://doi.org/10.1002/2014GL060197

Becherer, J., & Moum, J. N. (2017). An efficient scheme for onboard reduction of moored χpod data. *Journal of Atmospheric and Oceanic Technology*, *34*(11), 2533–2546.

Bhat, G., Gadgil, S., Kumar, P. H., Kalsi, S., Madhusoodanan, P., Murty, V., et al. (2001). Bobmex: The Bay of Bengal monsoon experiment. *Bulletin of the American Meteorological Society*, *82*(10), 2217–2243.

Chaudhuri, D., Sengupta, D., DAsaro, E., Venkatesan, R., & Ravichandran, M. (2019). Response of the salinity-stratified bay of bengal to cyclone phailin. *Journal of Physical Oceanography*. https://doi.org/10.1175/JPO-D-18-0051.1.

Fairall, C. W., Bradley, E. F., Hare, J. E., Grachev, A. A., & Edson, J. B. (2003). Bulk parameterization of air-sea fluxes: Updates and verification for the COARE algorithm. *Journal of Climate*, *16*(4), 571–591.

Fu, X., Wang, B., Li, T., & McCreary, J. P. (2003). Coupling between northwardpropagating, intraseasonal oscillations and sea surface temperature in the Indian Ocean. *Journal of the Atmospheric Sciences*, *60*(15), 1733–1753.

Girishkumar, M., Suprit, K., Chiranjivi, J., Bhaskar, T. U., Ravichandran, M., Shesu, R. V., & Rao, E. P. R. (2014). Observed oceanic response to tropical cyclone Jal from a moored buoy in the south-western Bay of Bengal. *Ocean Dynamics*, *64*(3), 325–335.

Gregg, M., D'Asaro, E., Riley, J., & Kunze, E. (2018). Mixing efficiency in the ocean. *Annual Review of Marine Science*, *10*, 443–473.
Hosom, D. S., Weller, R. A., Payne, R. E., & Prada, K. E. (1995). The IMET (improved meteorology) ship and buoy systems. *Journal of Atmospheric and Oceanic Technology*, *12*(3), 527–540.
Hoyos, C. D., & Webster, P. J. (2007). The role of intraseasonal variability in the nature of Asian monsoon precipitation. *Journal of Climate*, *20*(17), 4402–4424.
Inness, P. M., & Slingo, J. M. (2003). Simulation of the Madden-Julian oscillation in a coupled general circulation model. Part I: Comparison with observations and an atmosphere-only GCM. *Journal of Climate*, *16*(3), 345–364.
Jensen, T. G. (2003). Cross-equatorial pathways of salt and tracers from the northern Indian Ocean: Modelling results. *Deep Sea Research Part II: Topical Studies in Oceanography*, *50*(12–13), 2111–2127.
Jourdain, N. C., Lengaigne, M., Vialard, J., Madec, G., Menkes, C. E., Vincent, E. M., et al. (2013). Observation-based estimates of surface cooling inhibition by heavy rainfall under tropical cyclones. *Journal of Physical Oceanography*, *43*(1), 205–221.
Li, Y., Han, W., Ravichandran, M., Wang, W., Shinoda, T., & Lee, T. (2017). Bay of Bengal salinity stratification and Indian summer monsoon intraseasonal oscillation: 1. Intraseasonal variability and causes. *Journal of Geophysical Research: Oceans*, *122*, 4291–4311. https://doi.org/10.1002/2017JC012692
Lorbacher, K., Dommenget, D., Niiler, P., & Köhl, A. (2006). Ocean mixed layer depth: A subsurface proxy of ocean-atmosphere variability. *Journal of Geophysical Research*, *111*. C07010. https://doi.org/10.1029/2003JC002157
McDougall, T. J., & Barker, P. M. (2011). Getting started with TEOS-10 and the Gibbs Seawater (GSW) oceanographic toolbox. *SCOR/IAPSO WG*, *127*, 1–28.
McPhaden, M., & Foltz, G. (2013). Intraseasonal variations in the surface layer heat balance of the central equatorial Indian Ocean: The importance of zonal advection and vertical mixing. *Geophysical Research Letters*, *40*, 2737–2741. https://doi.org/10.1002/grl.50536
Moum, J. N. (2015). Ocean speed and turbulence measurements using Pitot-static tubes on moorings. *Journal of Atmospheric and Oceanic Technology*, *32*(7), 1400–1413.
Moum, J. N, de Szoeke, S. P., Smyth, W. D., Edson, J. B., DeWitt, H. L., Moulin, A. J., et al. (2014). Air-sea interactions from westerly wind bursts during the November 2011 MJO in the Indian Ocean. *Bulletin of the American Meteorological Society*, *95*(8), 1185–1199.
Moum, J. N., & Nash, J. D. (2009). Mixing measurements on an equatorial ocean mooring. *Journal of Atmospheric and Oceanic Technology*, *26*(2), 317–336.
Moum, J. N., Perlin, A., Nash, J. D., & McPhaden, M. J. (2013). Seasonal sea surface cooling in the equatorial Pacific cold tongue controlled by ocean mixing. *Nature*, *500*(7460), 64–67.
Moum, J. N., Pujiana, K., Lien, R.-C., & Smyth, W. D. (2016). Ocean feedback to pulses of the Madden-Julian oscillation in the equatorial Indian Ocean. *Nature Communications*, *7*, 13203.
Osborn, T. R. (1980). Estimates of the local rate of vertical diffusion from dissipation measurements. *Journal of Physical Oceanography*, *10*(1), 83–89.
Osborn, T. R., & Cox, C. S. (1972). Oceanic fine structure. *Geophysical & Astrophysical Fluid Dynamics*, *3*(1), 321–345.
Papa, F., Durand, F., Rossow, W. B., Rahman, A., & Bala, S. K. (2010). Satellite altimeter-derived monthly discharge of the Ganga-Brahmaputra river and its seasonal to interannual variations from 1993 to 2008. *Journal of Geophysical Research*, *115*. C12013. https://doi.org/10.1029/2009JC006075
Perlin, A., & Moum, J. N. (2012). Comparison of thermal variance dissipation rates from moored and profiling instruments at the equator. *Journal of Atmospheric and Oceanic Technology*, *29*(9), 1347–1362.
Pujiana, K., Moum, J. N., & Smyth, W. D. (2018). The role of turbulence in redistributing upper-ocean heat, freshwater, and momentum in response to the MJO in the Equatorial Indian Ocean. *Journal of Physical Oceanography*, *48*(1), 197–220.
Pujiana, K., Moum, J. N., Smyth, W. D., & Warner, S. J. (2015). Distinguishing ichthyogenic turbulence from geophysical turbulence. *Journal of Geophysical Research: Oceans*, *120*, 3792–3804. https://doi.org/10.1002/2014JC010659
Rajeevan, M., Gadgil, S., & Bhate, J. (2010). Active and break spells of the Indian summer monsoon. *Journal of Earth System Science*, *119*(3), 229–247.
Risien, C. M., & Chelton, D. B. (2008). A global climatology of surface wind and wind stress fields from eight years of quikscat scatterometer data. *Journal of Physical Oceanography*, *38*(11), 2379–2413.
Sengupta, D., Bharath Raj, G., Ravichandran, M., Sree Lekha, J., & Papa, F. (2016). Near-surface salinity and stratification in the north Bay of Bengal from moored observations. *Geophysical Research Letters*, *43*, 4448–4456. https://doi.org/10.1002/2016GL068339
Sengupta, D., Bharath Raj, G., & Shenoi, S. (2006). Surface freshwater from Bay of Bengal runoff and Indonesian throughflow in the tropical Indian Ocean. *Geophysical Research Letters*, *33*. L22609. https://doi.org/10.1029/2006GL027573
Sengupta, D., & Ravichandran, M. (2001). Oscillations of Bay of Bengal sea surface temperature during the 1998 summer monsoon. *Geophysical Research Letters*, *28*(10), 2033–2036. https://doi.org/10.1029/2000GL012548
Shetye, S., Gouveia, A., Shankar, D., Shenoi, S., Vinayachandran, P., Sundar, D., et al. (1996). Hydrography and circulation in the western bay of bengal during the northeast monsoon. *Journal of Geophysical Research*, *101*(C6), 14,011–14,025.
Shroyer, E. L., Rudnick, D. L., Farrar, J. T., Lim, B., Venayagamoorthy, S. K., St. Laurent, L. C., et al. (2016). Modification of upper-ocean temperature structure by subsurface mixing in the presence of strong salinity stratification. *Oceanography*, *29*(2), 62–71.
Smyth, W., Moum, J. N., & Caldwell, D. (2001). The efficiency of mixing in turbulent patches: Inferences from direct simulations and microstructure observations. *Journal of Physical Oceanography*, *31*(8), 1969–1992.
Sree Lekha, J., Buckley, J., Tandon, A., & Sengupta, D. (2018). Subseasonal dispersal of freshwater in the northern Bay of Bengal in the 2013 summer monsoon season. *Journal of Geophysical Research: Oceans*, *123*, 6330–634. https://doi.org/10.1029/2018JC014181
Sutherland, G., Marié, L., Reverdin, G., Christensen, K. H., Broström, G., & Ward, B. (2016). Enhanced turbulence associated with the diurnal jet in the ocean surface boundary layer. *Journal of Physical Oceanography*, *46*(10), 3051–3067.
Taylor, G. I. (1938). The spectrum of turbulence. Proceedings of the Royal Society of London A: Mathematical. *Physical and Engineering Sciences*, *164*, 476–490.
Warner, S. J., Becherer, J., Pujiana, K., Shroyer, E. L., Ravichandran, M., Thangaprakash, V., & Moum, J. N. (2016). Monsoon mixing cycles in the Bay of Bengal: A year-long subsurface mixing record. *Oceanography*, *29*(2), 158–169.
Weller, R. A., Farrar, J. T., Buckley, J., Mathew, S., Venkatesan, R., Sree Lekha, J., et al. (2016). Air-sea interaction in the Bay of Bengal. *Oceanography*, *29*(2), 28–37.
Weller, R., Farrar, J., Seo, H., Prend, C., Sengupta, D., Sree Lekha, J., et al. (2018). Moored observations of the surface meteorology and air-sea fluxes in the northern Bay of Bengal in 2015. *Journal of Climate*, *32*, 549–573.
Woolnough, S., Vitart, F., & Balmaseda, M. (2007). The role of the ocean in the Madden-Julian oscillation: Implications for MJO prediction. *Quarterly Journal of the Royal Meteorological Society*, *133*(622), 117–128.

References from Supporting Information

Lilly, J. M., & Olhede, S. C. (2010). On the analytic wavelet transform. *IEEE Transactions on Information Theory*, *56*(8), 4135–4156.
Lilly, J. M., & Olhede, S. C. (2012). Generalized Morse wavelets as a superfamily of analytic wavelets. *IEEE Transactions on Signal Processing*, *60*(11), 6036–6041.
Olhede, S. C., & Walden, A. T. (2002). Generalized Morse wavelets. *IEEE Transactions on Signal Processing*, *50*(11), 2661–2670.
Upper Ocean Data (2018). https://doi.org/10.6084/m9.figshare.7416440
Upper Ocean Processes Group (2016). http://uop.whoi.edu/projects/Bengal/